Interacting particles on a rocked ratchet: Rectification by condensation

Sergey Savel'ev,[1] Fabio Marchesoni,[1,2] and Franco Nori[1,3]

[1]*Frontier Research System, The Institute of Physical and Chemical Research (RIKEN), Wako-shi, Saitama 351-0198, Japan*
[2]*Dipartimento di Fisica, Università di Camerino, I-62032 Camerino, Italy*
[3]*Department of Physics, Center for Theoretical Physics, University of Michigan, Ann Arbor, Michigan 48109-1120, USA*
(Received 11 April 2004; revised manuscript received 29 October 2004; published 14 January 2005)

The transport of interacting particles subject to an external low-frequency ac force on a ratchetlike asymmetric substrate is studied via a nonlinear Fokker-Planck equation as well as via numerical simulations. With increasing the particle density, the ratchet current can either increase or decrease depending on the temperature, the drive amplitude, and the nature of the interparticle interaction. At low temperatures, attracting particles can condense randomly at some potential minima, thus breaking the discrete translational symmetry of the substrate. Depending on the drive amplitude, condensation results either in a drop to zero or in the saturation of the net particle velocity at densities above the condensation density—the latter case producing a very efficient rectification mechanism.

INTRODUCTION

Stochastic transport on periodic asymmetric (ratchet) substrates far from equilibrium has raised widespread interest in the recent literature [1]. Intense research activity in this field is partly motivated by the challenge to describe and control some biological processes at both the cell level (for instance, transport in ion channels [2]) and the body level (muscle operations [3]). Moreover, recent technological advances allow us to develop devices to guide tiny particles on nano- and microscales [4]. Some of these devices have already been realized experimentally to control the motion of vortices in superconductors [5], particles in asymmetric silicon pores [6], charged particles through artificial pores [7], and arrays of optical tweezers [8], among others.

An important implementation of this category of devices is the so-called rocked ratchet [9], where the oscillating particle motion driven by an external periodic force develops a net drift component due to the asymmetry of the substrate potential. It was proven analytically in 1D [9] and found numerically in 2D [10] that the net drift velocity in a ratchet exhibits a maximum versus the driving amplitude (or the temperature). This allows us in some cases to tune the dc ratchet output to a desired value. However, the far-less-studied *interaction* among particles is expected to have an important role in the rectification power of a rocked ratchet. Indeed, it has already been found [10–16] that interactions can result in very unusual transport properties, including spontaneous symmetry breaking, commensurability effects, unusual negative mobility, and surprising current inversions.

This paper analyzes the density dependence of the ratchet current of a 1D gas of interacting particles. We stress that this model can describe a variety of physical systems [4]. For instance, experiments on transport in an ion channel [2,17] and particles in asymmetric silicon pores [6] could be studied theoretically within the model discussed in this paper. Moreover, a similar model [18] was successfully used for interpretating the net motion of vortices in a magnetic-superconductor hybrid microstructure [5]. In particular, when increasing the vortex density (magnetic field), a current inversion was predicted and observed [5].

The apparently simple model studied here is very hard to investigate analytically. We study it by solving a nonlinear Fokker-Planck equation, where the interparticle interaction is effectively accounted for by means of a mean-field potential [18]. Our analytical results are confirmed through numerical simulations, which, in turn, allow us to reach beyond the mean-field approximation. For repulsive interactions, we show that the particle net current hits a maximum when increasing the particle density at relatively low temperatures and drive amplitudes; otherwise, it gets monotonously suppressed as the density increases. In contrast, for attracting particles, the net current grows with increasing their density n up to a certain value n_c, where the analytical solution to our mean-field scheme indicates the occurrence of a *drive-dependent dynamical phase transition*. Extensive numerical simulations prove that, for a low ac amplitude, the particles condense around the potential minima as they are being pushed in either direction. This results in the *sudden drop of their drift velocity at the condensation point*. On raising the drive amplitude, it can happen that the particles condense only when the ac force pushes them against the steeper slope of the asymmetric substrate wells, while remaining in the running state as they are driven in the opposite direction. For such a range of large drive amplitudes, *the ratchet current versus the particle density saturates at a maximal value in the vicinity of the condensation density.*

MODEL

Langevin and Fokker-Planck approaches

Our starting point is the set of Langevin equations

$$\dot{x}_i = -\frac{\partial U(x_i)}{\partial x_i} - \sum_{j \neq i} \frac{\partial}{\partial x_i} W(x_i - x_j) + F(t) + \sqrt{2k_B T} \xi^{(i)}(t) \quad (1)$$

for interacting particles moving on the one-dimensional asymmetric periodic potential U, $U(x+l)=U(x)$, in the presence of a time-periodic force $F(t)$ with frequency ν. Here, the Gaussian white noise $\xi^{(i)}(t)$ with zero average $\langle \xi^{(i)} \rangle = 0$

satisfies the fluctuation-dissipation relation $\langle \xi^{(i)}(t)\xi^{(i)}(t+\tau)\rangle = \delta(\tau)\delta$; T is the temperature, k_B is the Boltzmann constant, and W denotes the pair interaction potential. Indices i and j run over all particles. For simplicity, we set the viscous coefficient equal to 1 (Smoluchowski approximation). We integrated the equation set (1) for our numerical simulations, while the analytical predictions reported below were derived by solving the integro-differential equations for the corresponding many-particle distribution functions. The Fokker-Planck-like equation for the one-particle distribution function, $F_1(t,x)$, can be written in the form [19]

$$\frac{\partial F_1(t,x)}{\partial t} = \frac{\partial}{\partial x}\left[\left(\frac{\partial U(x)}{\partial x} - F(t)\right)F_1(t,x)\right] + \frac{\partial}{\partial x}F_1(t,x)$$
$$\times \int d\tilde{x}\, F_1(t,\tilde{x})\, G(t,x,\tilde{x})\frac{\partial W(x-\tilde{x})}{\partial x} + k_BT\frac{\partial^2 F_1(t,x)}{\partial x^2}, \qquad (2)$$

where $F_2(t,x,\tilde{x}) \equiv F_1(t,x)F_1(t,\tilde{x})G(x,\tilde{x},t)$ denotes a binary distribution function. It is apparent that particle-particle correlations decay on a scale of the order of either the interaction length λ for low particle densities, $n \ll 1/\lambda$, or the interparticle distance $1/n$ for high particle densities, $n \gg 1/\lambda$. As a consequence, the function G, which describes the particle-particle correlation, differs appreciably from 1 (uncorrelated particle motion) for particle separations $|x-\tilde{x}| \lesssim \min\{n^{-1},\lambda\}$, only. This has been numerically proved in [19]. Therefore, if each particle interacts with many neighbors, i.e., $n\lambda \gg 1$, the function G in Eq. (2) can be safely approximated to 1 over the entire integration domain (of order λ) of $\int d\tilde{x}F_1 G\partial W/\partial x$. It follows that Eq. (2) can be reduced to its *mean-field* form [18–20]

$$\frac{\partial F_1(t,x)}{\partial t} = -\frac{\partial j}{\partial x}$$
$$= \frac{\partial}{\partial x}\left[F_1(t,x)\left\{\frac{\partial U^{\mathrm{mf}}}{\partial x} - F(t)\right\} + k_BT\frac{\partial F_1(t,x)}{\partial x}\right], \qquad (3)$$

where the mean-field potential $U^{\mathrm{mf}}(x)$ is defined as

$$U^{\mathrm{mf}}(x) = U(x) + \int dx'\, W(x-x')F_1(t,x'). \qquad (4)$$

Hereafter, the one-particle distribution function $F_1(t,x)$ is normalized in terms of the average particle density n, i.e.,

$$\int_0^l F_1(t,x)\, dx/l = n. \qquad (5)$$

In order to make the problem more tractable, we further discard nonlocal effects by assuming the interaction length λ to be much smaller than the period l of the substrate potential $U(x)$. This allows us to replace the integro-differential equation (3) by

$$\frac{\partial F_1(t,x)}{\partial t} = \frac{\partial}{\partial x}\left[\left(\frac{\partial U(x)}{\partial x} - F(t)\right)F_1(t,x) + gF_1\frac{\partial F_1}{\partial x}\right]$$
$$+ k_BT\frac{\partial^2 F_1(t,x)}{\partial x^2} \qquad (6)$$

with

$$g \equiv \int dx'\, W(x-x'). \qquad (7)$$

Therefore, Eq. (6) is valid under the following restrictions:

$$n^{-1} \ll \lambda \ll l. \qquad (8)$$

Note that, even though we assumed locality with respect to the substrate unit length, the interparticle interaction can still be regarded as a long-range interaction because of the density requirement $\lambda \gg 1/n$. These are the approximations under which in the following sections we solve analytically Eq. (6) and compare our analytical results with data from numerical simulations based on the Langevin equations (1). Although conditions (8) strictly apply to a limited class of physical systems, the results obtained below have much wider applicability. Indeed, numerical simulations performed well outside the parameter region (8) agree quite closely with our mean-field description.

Adiabatic approximation

In the low-frequency limit, at any time t_0 the system can be regarded as being in the steady state corresponding to an applied dc force $F \equiv F(t_0)$; hence, the adiabatic expression for the ratchet current

$$j_{\mathrm{DC}} = \nu \int_0^{1/\nu} j(F)\, dt_0, \qquad (9)$$

where $j(F)$ is the stationary current in the presence of the constant drive F. If $j(F)$ is not an odd function of F, then the rocked ratchet can rectify the oscillatory motion of the particles. The stationary solution to Eq. (3) can be written as

$$-j(F) = (U' - F)F_1(x) + k_BTF_1' + gF_1F_1' \qquad (10)$$

(the prime denotes an x derivative). When adopting, for simplicity, the piecewise linear periodic potential [inset in Fig. 1(a)]

$$U = Q\frac{x}{l_1} \quad \text{for } 0 < x < l_1,$$

$$U = Q\left[1 - \frac{x-l_1}{l_2}\right] \quad \text{for } l_1 < x < l \qquad (11)$$

($l_1+l_2 \equiv l$), the stationary one-particle distribution in Eq. (10), $F_1(x)$, can be expressed in implicit form as

$$\frac{F_1(F-f_1)-j}{P_0(F-f_1)-j} = \exp\left(\frac{(F-f_1)x - g(F_1-P_0)}{k_BT + gj/(F-f_1)}\right) \qquad (12)$$
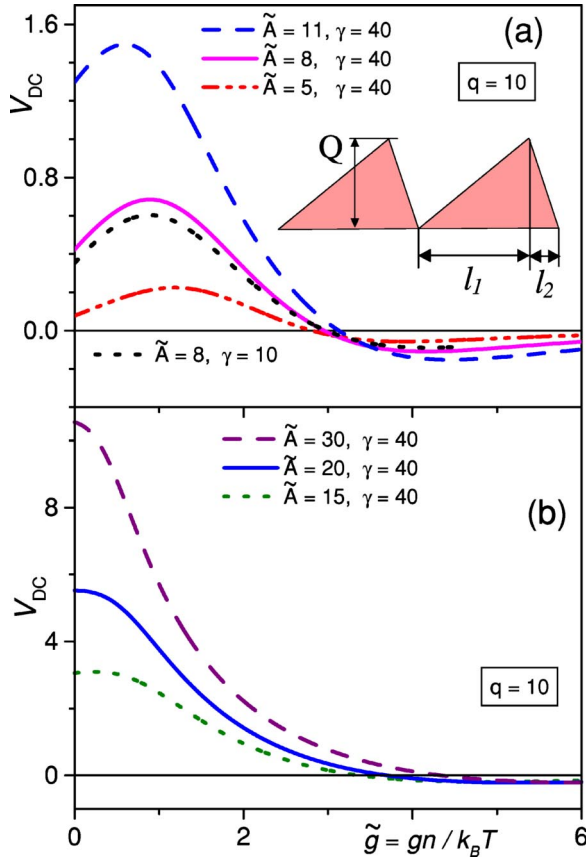
for $0 < x < l_1$, and

FIG. 1. (Color online) Repelling particles: net velocity V_{DC} versus dimensionless pair coupling $\tilde{g}=gn/k_BT$ for different values of $\tilde{A}$ in the regime of high activation, $q=Q/k_BT=10$, and large anisotropy γ. $V_{DC}(\tilde{g})$ exhibits a broad peak for $\tilde{A}<20$. The normalized driving amplitude $\tilde{A}=lA/k_BT$ is a measure of the strength of the ac drive, compared to the disordering thermal energy. These results were obtained by solving the mean-field set of equations [Eq. (14)]. Inset in (a): two cells of the sawtooth substrate potential [Eq. (11)].

$$\frac{F_1(F+f_2)-j}{P_1(F+f_2)-j}=\exp\left(\frac{(F+f_2)(x-l_1)-g(F_1-P_1)}{k_BT+gj/(F+f_2)}\right) \quad (13)$$

for $l_1<x<l$. Here, P_0 and P_1 are the particle densities at the potential minima and maxima, respectively, i.e., $P_0=F_1(0)$, $P_1=F_1(l_1)$; $f_1=Q/l_1$ and $f_2=Q/l_2$ are the two restoring forces exerted by the substrate.

Two equations for the three unknown quantities P_0, P_1, and j were derived writing Eqs. (12) and (13) for the extremal points $x=l_1$ and $x=l$, respectively, and imposing periodic boundary conditions $F_1(l)=F_1(0)=P_0$. A third equation for these variables was obtained by integrating Eq. (10) over one unit cell of the piecewise linear potential $U(x)$ and then eliminating the two integration constants $\int_0^{l_1}F_1(x)dx$ and $\int_{l_1}^l F_1(x)dx$ by means of the normalization condition (5). The resulting equations can be conveniently expressed as

$$\mathcal{P}-\frac{V}{f^-}=-\frac{\Delta}{2}\coth\left\{\frac{f^-/\Gamma_1+\tilde{g}\Delta}{2[1+\tilde{g}V/f^-]}\right\},$$
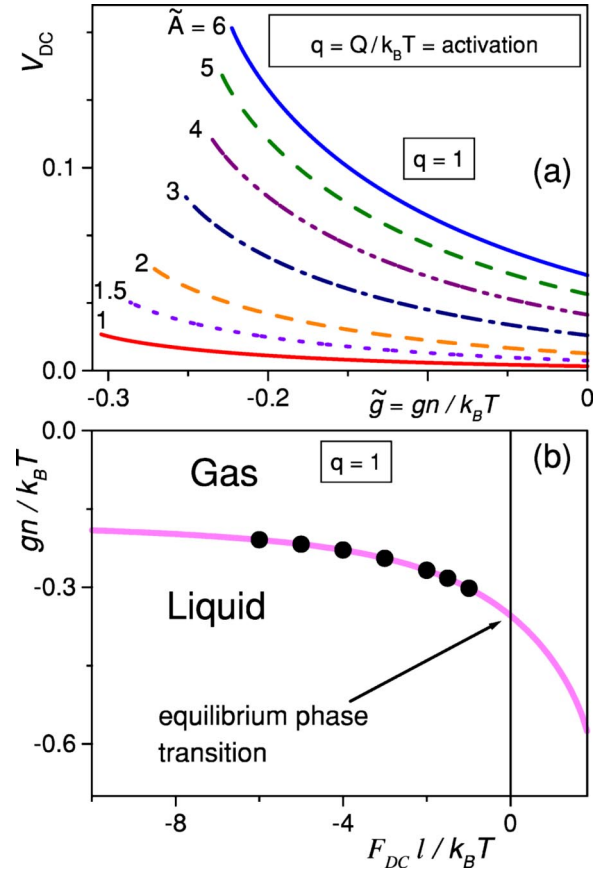
FIG. 2. (Color online) Attracting particles: (a) Net velocity V_{DC} versus effective interaction coupling $\tilde{g}=gn/k_BT$ for different values of driving amplitudes $\tilde{A}=Al/k_BT$ in the regime of low activation, $q=1$, and large anisotropy, $\gamma=40$. There exists no mean-field solution for $\tilde{g}<\tilde{g}_c$ (left end points). (b) Gas-liquid phase diagram in the density-drive plane. The phase boundary between gas and liquid phases was obtained based on the criterion of existence of a solution to the mean-field equations (14). At zero driving $F_{DC}=0$, the transition is an equilibrium transition. The condensation transition is driven out of equilibrium by increasing the DC force F_{DC}. Black dots in (b) mark the left-end-points of curves in (a). These results were obtained by solving the mean-field set of equations (14).

$$\mathcal{P}-\frac{V}{f^+}=\frac{\Delta}{2}\coth\left\{\frac{f^+/\Gamma_2-\tilde{g}\Delta}{2[1+\tilde{g}V/f^+]}\right\},$$

$$V=\frac{f^-f^++(\tilde{g}\mathcal{P}+1)\Delta q\Gamma_1\Gamma_2}{f+q(\Gamma_2-\Gamma_1)}, \quad (14)$$

in terms of the dimensionless variables

$$\mathcal{P}=\frac{P_0+P_1}{2n},$$

$$\Delta=\frac{P_0-P_1}{n},$$

$$V=\frac{jl}{k_BTn}, \quad (15)$$

and the model parameters

$$q = \frac{Q}{k_B T} = \text{(activation)},$$

$$f = \frac{Fl}{k_B T} = \text{(drive)},$$

$$\tilde{g} = \frac{gn}{k_B T} = \text{(density or pair coupling), and}$$

$$\gamma = l_1/l_2 = \text{(ratchet anisotropy).} \tag{16}$$

Here, we introduced the auxiliary anisotropy parameters

$$\Gamma_1 = l/l_1 = 1 + \gamma^{-1} \text{ and}$$

$$\Gamma_2 = l/l_2 = 1 + \gamma, \tag{17}$$

as well as the total dimensionless forces

$$f^- = f - q\Gamma_1 \text{ and}$$

$$f^+ = f + q\Gamma_2 \tag{18}$$

experienced by a single particle moving along the relevant sides of a potential well. A crucial assumption of this analytical procedure is the spatial periodicity of the distribution function $F(x) = F(x+l)$. This allowed us to reduce a spatially infinite problem to one cell (say, from x to $x+l$). However, this simplification becomes invalid near the condensation transition, where a spontaneous symmetry breaking mechanism destroys the translational symmetry of the substrate cells.

At low densities, the net particle velocity can be expanded in powers of $\tilde{g}$,

$$V = V_0 + \tilde{g} V_1 + \mathcal{O}(\tilde{g}^2), \tag{19}$$

where V_0 and V_1 read

$$V_0(f) = \frac{(f^- f^+)^2 \alpha}{f^- f^+ [f + q(\Gamma_2 - \Gamma_1)]\alpha - 2(q\Gamma_1\Gamma_2)^2}, \tag{20}$$

$$V_1(f) = \frac{q\Delta_0\Gamma_1\Gamma_2 f^- f^+ \{\mathcal{P}_0\alpha - [\Delta_0 + V_0/\Gamma_2]\beta^+ + [\Delta_0 - V_0/\Gamma_1]\beta^-\}}{f^- f^+ [f + q(\Gamma_2 - \Gamma_1)]\alpha - 2(q\Gamma_1\Gamma_2)^2}, \tag{21}$$

respectively. Here, we used the zeroth-order approximation of the dimensionless probabilities

$$\Delta_0 = \Delta(\tilde{g} = 0) = \frac{[f + q(\Gamma_2 - \Gamma_1)]V_0 - f^- f^+}{q\Gamma_1\Gamma_2},$$

$$\mathcal{P}_0 = \mathcal{P}(\tilde{g} = 0) = \frac{\Delta_0}{2} \coth\left[\frac{f^+}{2\Gamma_2}\right] + \frac{V_0}{f^+}, \tag{22}$$

and the following combinations of Boltzmann-like prefactors:

$$\alpha = \coth\left(\frac{f^+}{2\Gamma_2}\right) + \coth\left(\frac{f^-}{2\Gamma_1}\right),$$

$$\beta^+ = \left[2\sinh^2\left(\frac{f^+}{2\Gamma_2}\right)\right]^{-1},$$

$$\beta^- = \left[2\sinh^2\left(\frac{f^-}{2\Gamma_1}\right)\right]^{-1}. \tag{23}$$

The functions $\Delta(\tilde{g})$, $P(\tilde{g})$, and $V(\tilde{g})$ at small $\tilde{g}$ can be determined by means of Eqs. (20) and (21). In order to compute these functions at higher $\tilde{g}$, Eqs. (14) can be solved numerically by increasing $\tilde{g}$ stepwise through a simple iteration procedure. Numerically obtained curves for $V(\tilde{g})$ are plotted in Figs. 1 and 2.

ANALYTICAL RESULTS

Let us now consider the square-wave signal $F(t) = A \, \text{sgn}[\cos(2\pi\nu t)]$ with $\text{sgn}[\cdots]$ denoting the sign of the argument. In the adiabatic approximation with frequency $\nu \ll A/l$, the particle net velocity can be written as

$$V_{\text{DC}} = [V(\tilde{A}) + V(-\tilde{A})]/2, \tag{24}$$

where $V(\pm\tilde{A})$ are the relevant drift velocities in the presence of the dc forces $\pm\tilde{A}$, respectively, with

$$\tilde{A} \equiv \frac{lA}{k_B T}. \tag{25}$$

The $\tilde{g}$ dependence of V_{DC} is shown in Fig. 1(a) for the case of repelling particles in the regime of large activations q (i.e., a large ratio of the potential barrier to thermal-fluctuation energy). Particle transport in the ratchet is enhanced by increasing the interaction strength g (or the particle density n) at relatively low drives $\tilde{A}$, as shown by the pronounced maxima of the corresponding curves $V_{\text{DC}}(\tilde{g})$ at $\tilde{g} > 0$ [Fig. 1(a)]. This effect is suppressed for larger values of $\tilde{A}$, where a monotonic decay of $V_{\text{DC}}(\tilde{g})$ was observed [Fig. 1(b)]. The dependence of V_{DC} on $\tilde{g}$ and $\tilde{A}$ can be understood qualitatively by noticing that the repelling particles tend to expel one another from the potential wells; this effectively smoothes out the potential barriers. For high q and low drives $\tilde{A}$, the particles are strongly confined in the potential
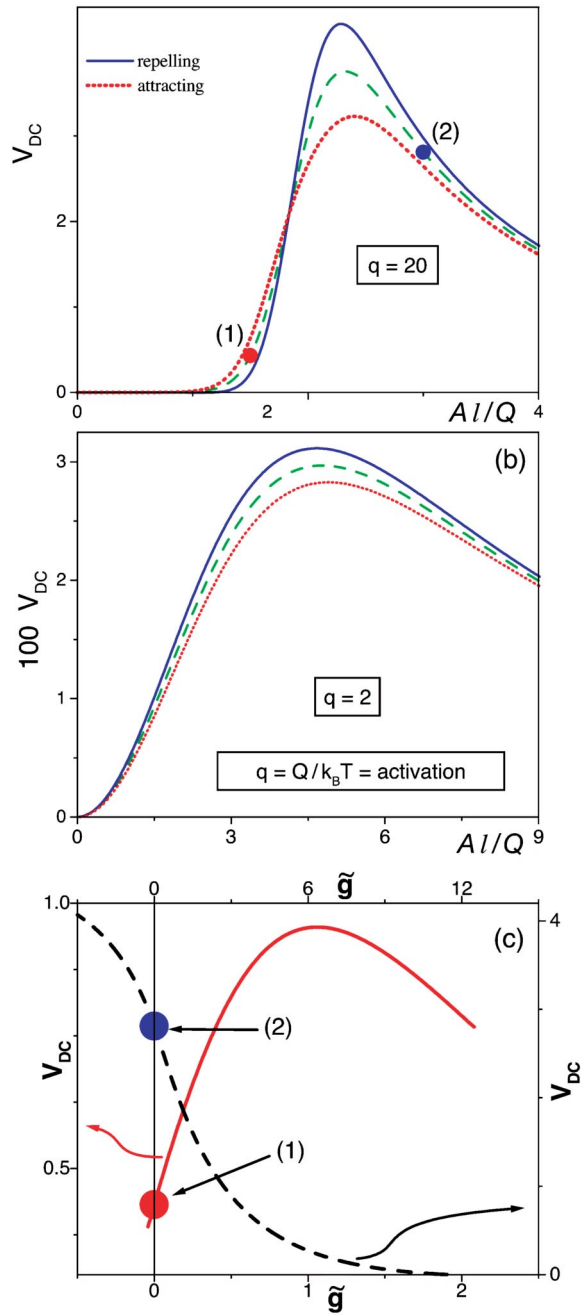
FIG. 3. (Color online) Net particle speed V_{DC} versus drive amplitude A for repelling, attracting, and noninteracting particles at $\gamma=1.2$, $\tilde{g}=\pm0.05$, $q=20$ (a) and $q=2$ (b). Panel (c) shows the curves V_{DC} versus effective interaction strength $\tilde{g}$ for the parameter values corresponding to the dots (1) and (2) in (a). These results were obtained by solving the mean-field set of equations (14).

wells so that the drift current is weak. In such a case, the suppression of the potential barriers due to the mutual repulsion of the particles enhances their mobility, thus allowing a stronger rectification effect. However, at even stronger drives, $\tilde{A}\gtrsim q$, the suppression of the barriers, when $\tilde{g}$ increases, results in a weaker anisotropy of the system: The positive and negative currents compensate each other more effectively, leading to a monotonic decay of $V_{DC}(\tilde{g})$. For low
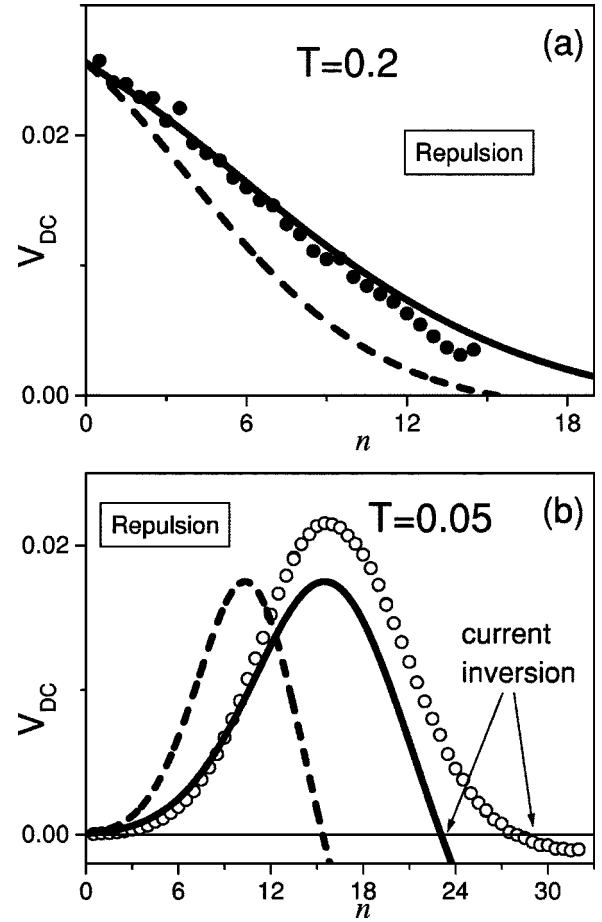

FIG. 4. V_{DC} versus n for repelling particles. These data (symbols) were obtained by numerically solving the Langevin Eq. (1) for the potential $U(x)$ in Eq. (11) and the truncated pair potential $W(x)$ in Eq. (27); while the analytical curves were obtained by solving the mean-field set of equations (14). Other simulation parameters: $\nu=0.01$, $A=0.5$, $Q=1$, $l_1=0.9$, $\lambda=0.1$, $g_{MD}=0.02$. (a) $T=0.2$ (solid circles) and (b) $T=0.05$ (open circles). Periodic boundary conditions were imposed over two unit cells of the piecewise linear potential (11). The corresponding analytical predictions for $g=g_{MD}=0.02$ (dashed lines) and $g=g_{MF}=0.02/1.5\approx0.0133$ (solid lines) are reported for comparison (see text).

barriers $q\lesssim1$, e.g., higher temperatures, the interval of the drive amplitude $\tilde{A}$, where $V_{DC}(\tilde{g})$ exhibits a peak [as in Fig. 1(a)], shrinks and finally disappears completely.

The case of attracting particles corresponds to negative values of the dimensionless pair coupling $\tilde{g}$. When $\tilde{g}$ is very small, V_{DC} is a linear function of $\tilde{g}$,

$$V_{DC}=[V_0(\tilde{A})+\tilde{g}V_1(\tilde{A})+V_0(-\tilde{A})+\tilde{g}V_1(-\tilde{A})]/2. \quad (26)$$

Thus, as opposed to the case of repelling particles, the net velocity V_{DC} increases [Fig. 2(a)] with increasing the particle density n or the strength $|g|$ of interactions for relatively low q values and/or large $\tilde{A}$. Similarly, V_{DC} decreases with increasing n or $|g|$ for large q [see Fig. 3(c), solid curve]. However, the applicability of these results for attractive interactions is restricted to the negative interval of $\tilde{g}$ extending
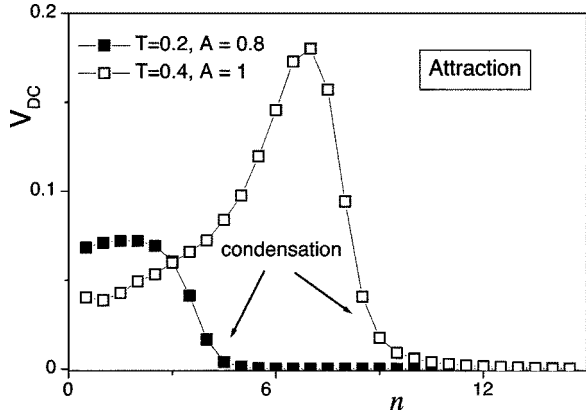
FIG. 5. V_{DC} versus n for attracting particles with $A=0.8$, $T=0.2$ (solid squares) and $A=1$, $T=0.4$ (open squares). Periodic boundary conditions were imposed over two unit cells of the piecewise linear potential (11). These results were obtained by numerically solving the Langevin Eq. (1) for the potential $U(x)$ in Eq. (11) and the truncated pair potential $W(x)$ in Eq. (27). Other simulation parameters: $\nu=0.01$, $Q=1$, $l_1=0.9$, $\lambda=0.1$, and $g=-0.02$.

from zero down to the critical value $\widetilde{g}_c(\widetilde{A}, q)$ (corresponding to a critical density n_c or a critical interaction strength g_c) for which Eq. (14) ceases to have a solution. This happens when the probability, $P_0=F_1(0)$, for the particles to sit at the bottom of the potential wells reaches a corresponding critical value, which for $\gamma \rightarrow \infty$ approaches $k_B T/|g|$. This behavior signals the onset of a phase transition: A macroscopic number of attracting particles is predicted to condense in the "liquid" phase around the substrate minima. Note that this finding for *long-range* interacting particles does not contradict the common understanding that such a phase transition cannot occur in a 1D multiparticle system with *short-range* interactions. Indeed, as mentioned above, the local form of the mean-field Fokker-Planck equation (6) was obtained under the assumption (8) that many particles can be fitted within one interaction length, so that their interactions can be regarded as long-range. Using the criterion of the existence of the mean-field solution Eq. (14), we constructed the boundary [Fig. 2(b)] between gaslike and liquidlike phase for attracting particles subjected to a dc force F_{DC}: The ensuing phase transition turns out to be sensitive also to the presence of external biases, i.e., the condensation point depends on F_{DC}, $n_c=n_c(F_{DC})$.

To determine the interval of driving amplitudes A where increasing the density n of the interacting particles enhances rectification, we computed the curves $V_{DC}(\widetilde{A})$ for small values of $\widetilde{g}$ using the analytical expressions (20) and (21) for V_0 and V_1 [Fig. 3(a)]. For high q, the net velocity of repelling particles increases (decreases) with increasing g (or n) if the drive is smaller (larger) than an optimal value [Fig. 3(a)]. For the same value of q, the current of attracting particles behaves in the opposite way. Two typical curves $V_{DC}(\widetilde{g})$, for fixed values of A and q, are displayed in Fig. 3(c). For low q, V_{DC} grows monotonically with $\widetilde{g}$, no matter what the value of A [i.e., V_{DC} increases (decreases) monotonically with raising n or changing g from negative (attracting) to positive values (repelling particles)]: The three curves $V_{DC}(A)$ plotted in Fig. 3(b) never cross.
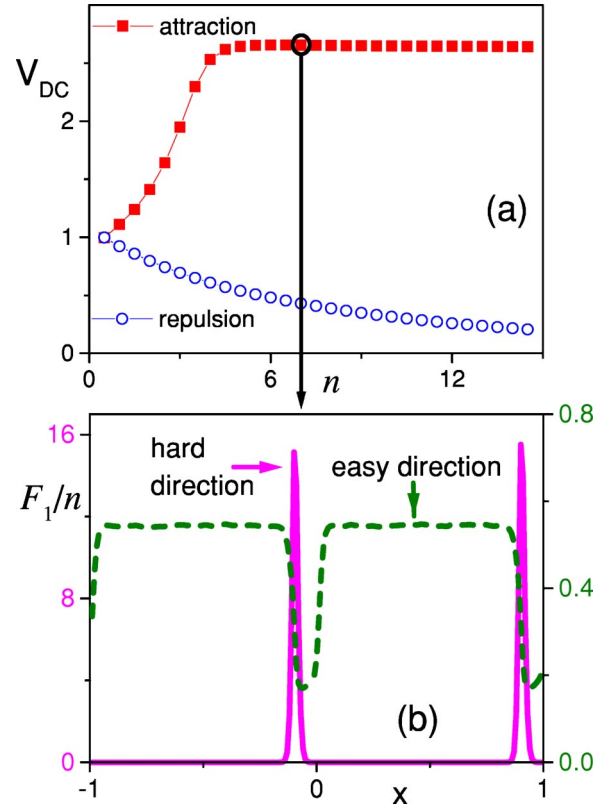

FIG. 6. (Color online) (a) Net average velocity V_{DC} versus particle density n for repelling (open circles) and attracting (solid squares) particles. These results were obtained by numerically solving the Langevin Eq. (1) for the potential $U(x)$ in Eq. (11) and the truncated pair potential $W(x)$ in Eq. (27). Other simulation parameters are $\nu=0.01$, $A=6$, $Q=1$, $l_1=0.9$, $\lambda=0.1$, $g=-0.02$, and $T=0.2$. (b) Spatial distribution of attracting particles for $n=7$, corresponding to data marked by a black circle in (a). One snapshot (normalized distribution $\equiv F_1/n$) of the particles was taken at each drive period with the external force pushing in the "hard" (solid line, the left axis) or the "easy" (dotted line, the right axis) direction, respectively. Particle condensation at both potential minima is apparent in the latter case. In both panels, periodic boundary conditions were imposed over two unit cells of the piecewise linear potential (11).

NUMERICAL SIMULATIONS

In order to assess our analytical predictions, we numerically simulated the Langevin dynamics (1) for the piecewise linear periodic potential $U(x)$ in Eq. (11) and a conveniently truncated pair potential

$$W(y) = g \frac{\lambda - |y|}{\lambda^2} \quad \text{if} \quad |y| < \lambda,$$

$$W = 0 \quad \text{otherwise.} \tag{27}$$

Figures 4(a) (solid symbols) and 4(b) (open circles) clearly show that, as predicted in our theoretical analysis, the net current for repelling particles increases (decreases) with the density at low (high) temperatures [high (low) q]. The comparison between numerics (dots) and theory (dashed curves)
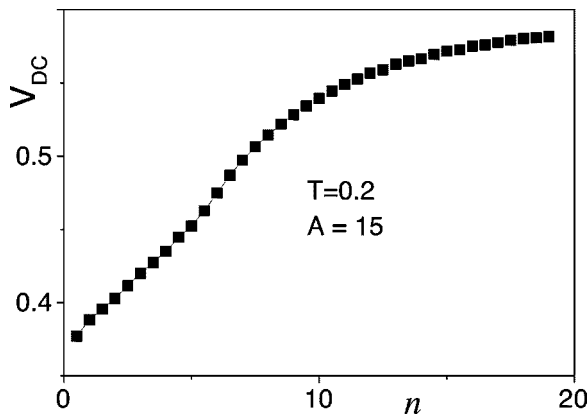
FIG. 7. Net velocity V_{DC} versus particle density n for attracting particles with $A=15$ and $T=0.2$. These results were obtained by numerically solving the Langevin Eq. (1) for the potential $U(x)$ in Eq. (11) and the truncated pair potential $W(x)$ in Eq. (27). Other simulation parameters are $\nu=0.01$, $Q=1$, $l_1=0.9$, $\lambda=0.1$, and $g=-0.02$. Periodic boundary conditions were imposed over two unit cells of the piecewise linear potential (11). Because of the strong driving, there is no condensation and V_{DC} increases monotonically.

reveals a quantitative disagreement. This apparent discrepancy points to unavoidable corrections to our mean-field scheme, including an appreciable screening [19] of the interparticle interaction, and nonlocality effects introduced by the truncated pair potential W used in the simulations. To make the approximate analytical curves reproduce closer the corresponding simulation data, the bare interaction constant $g=g_{MD}$ employed in the simulation must be replaced in Eqs. (14) by a rescaled interaction constant g_{MF}, namely $g_{MF} \simeq g_{MD}/1.5$ (solid curves versus circles in Fig. 4). Thus, our analytical results agree quite well with numerics, including the current inversion at high particle density in Fig. 4(b).

As predicted analytically, for the case of attracting particles, the ratchet current increases with the particle density up to the condensation point n_c [Figs. 5 and 6 (squares)]. For densities above the condensation threshold n_c, different scenarios can take place. If the amplitude A of the ac force is smaller than both substrate restoring forces Q/l_1 and Q/l_2, then the particles condense in the tilted potential wells, regardless of the orientation of the drive. Since the mobility of the condensed particles is zero, the average net particle current vanishes for $n > n_c$ (Fig. 5). Most notably, if A takes values between the two substrate forces Q/l_1, Q/l_2, i.e., $f_1 < A < f_2$, then potential wells can exist only in one tilted configuration (here, $U+Ax$). Therefore, in our simulation the particles condense at the minima of $U+Ax$, when the ac force pushes them to the left; the instantaneous current in such a "hard" direction drops to zero. On the contrary, the particles are almost ballistic when the periodic force pushes them in the opposite, "easy" direction (no minima and therefore no condensation in $U-Ax$). The stroboscopic spatial distribution of attracting particles subject to an ac drive pointing in the hard and easy directions, respectively, is shown in Fig. 6(b): When pushed in the hard direction, almost all particles condense at the bottom of the wells; on the contrary, particles moving to the right in the running state are distributed quite homogeneously in space. Therefore, motion is allowed in the
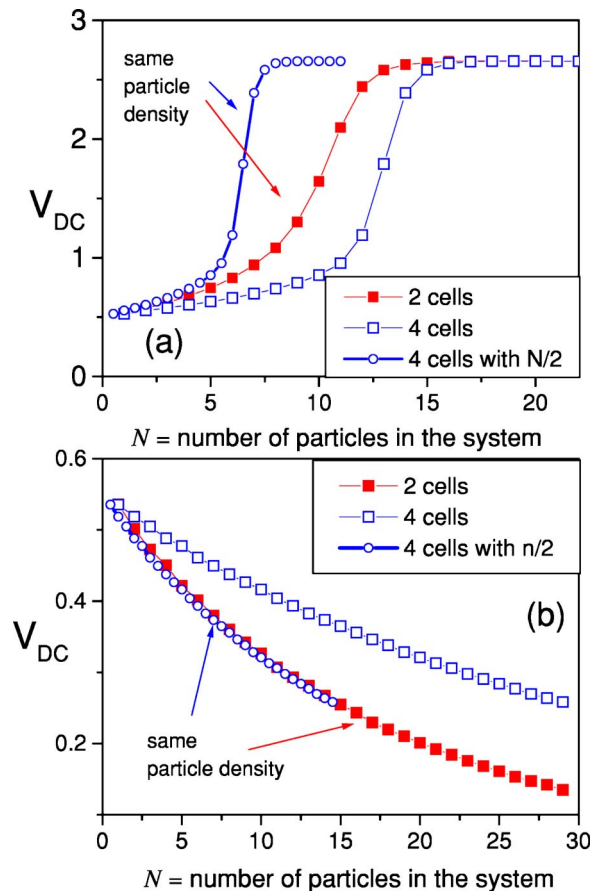

FIG. 8. (Color online) Net velocity V_{DC} versus the number of particles N for (a) attracting and (b) repelling particles. These results were obtained by numerically solving the Langevin Eq. (1) for the potential $U(x)$ in Eq. (11) and the truncated pair potential $W(x)$ in Eq. (27). Periodic boundary conditions were imposed over two (solid squares) and four potential unit cells (open squares). Other simulation parameters are $\nu=0.01$, $Q=1$, $l_1=0.9$, $\lambda=0.1$, $g=\pm0.02$, $T=0.3$, and $A=6$. The open small circles are the simulation data for a four-cell chain with half the number of particles, i.e., V_{DC} versus $N/2$.

"easy" or natural ratchet direction, only; the curve $V_{DC}(n)$ levels off in correspondence with the condensation density n_c, i.e., it *saturates* for $n > n_c$ [Fig. 6(a), squares]. For larger ac forces with $A > \max(f_1, f_2)$, no condensation occurs in either direction and $V_{DC}(n)$ approaches monotonically a saturation value (Fig. 7) which decreases with increasing A.

SPONTANEOUS SYMMETRY BREAKING

Next, we study how the net velocity V_{DC} depends on the total number N of particles in a periodic ratchet with a period of two or four unit cells (Fig. 8), i.e., two-teeth [inset in Fig. 1(a)] or four-teeth closed chains. These results can be easily extended for larger numbers of unit cells.

For repulsive particle-particle interactions, the net velocity $V_{DC}^{(4)}$ of the four-cell ratchet chain coincides with the net velocity $V_{DC}^{(2)}$ of the two-cell ratchet chain as long as the two devices support the same particle density: that is, $V_{DC}^{(4)}(2N)$
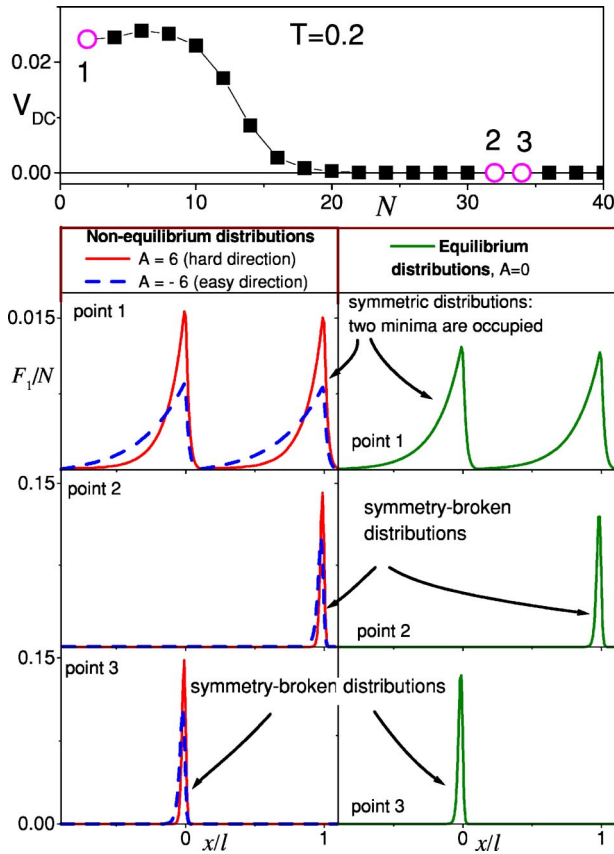
FIG. 9. (Color online) Spontaneous symmetry breaking destroys the equivalence of two neighboring potential cells at the phase transition. The normalized particle distributions $F_1(x/l)/N$ are shown for four different total numbers $N=2n$ of particles inside the two cells, corresponding to the net velocity $V_{DC}(N)$ shown at the top. The normalized equilibrium distributions $F_1(x/l)/N$ for the same particle numbers are also shown in the right column. These results were obtained by numerically solving the Langevin Eq. (1) for the potential $U(x)$ in Eq. (11) and the truncated pair potential $W(x)$ in Eq. (27). The parameters used here are $\nu=0.01$, $Q=1$, $l_1=0.9$, $\lambda =0.1$, $g=-0.02$, $T=0.2$, and $A=0.5$. Both cells are equally occupied at densities lower than the condensation point (e.g., point 1); this equivalence is broken at higher densities (point 2 and 3).

$=V_{DC}^{(2)}(N)$ [see Fig. 8(b)]. This means that the net velocities depend only on the particle density in the ratchet, as suggested by the spatial equivalence of the potential cells.

In contrast, for attracting particles, we obtain $V_{DC}^{(4)}(2N) \neq V_{DC}^{(2)}(N)$ [Fig. 8(a)], which indicates that the cell equivalence is broken. In order to clarify this property, we plot the particle distributions F_1 below and above the condensation point (Fig. 9). Simulating two substrate potential cells, we found that both cells are equivalently occupied at low particle densities (see point 1, below the condensation point). Above condensation (points 2 and 3), the spatial equivalence of the two cells is spontaneously broken: particles condense either on the right or the left minimum, no matter if the initial particle distribution was set the same in both cells. This is the manifestation of very small fluctuations getting strongly amplified in time. Note that the translational symmetry of the substrate may be broken in nonequilibrium (at
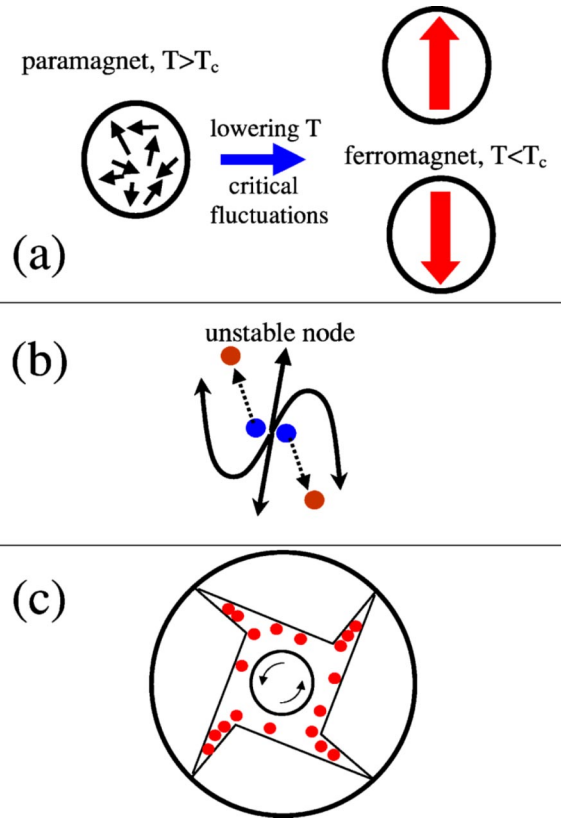

FIG. 10. (Color online) The mechanism of spontaneous symmetry breaking of Fig. 9 has counterparts in the theory of equilibrium phase transitions [e.g., the paramagnetic-ferromagnetic transition shown in (a) and certain dynamical instabilities of the type sketched in (b), see text]. (c) A schematic diagram of a simple realization of a four-cell ratchet device. Two coaxial cylinders, the outer one having a sawtooth-shaped inner cross section, rotate with angular frequency Ω_R; subject to the resulting centrifugal force, the elastic particles experience an effective ratchetlike potential. An ac driving force can be generated by periodically switching the rotation frequency between two values $\Omega_R \pm \Delta\Omega_R$.

relatively weak driving) and equilibrium operating conditions (no external drive) alike.

In the mean-field approach, this peculiar symmetry breaking can be understood as due to the competition of solutions with different spatial periods: l, $2l$, $3l$, etc. Indeed, for a two-cell chain, the analytical technique of Sec. II B would introduce five independent variables: $P_0=F_1(0)$, $P_1=F_1(l_1)$, $P_2=F_1(l)$, $P_3=F_1(l+l_1)$, and j, instead of the three variables $P_0=F_1(0)$, $P_1=F_1(l_1)$, and j in Eq. (14). In order to derive a complete set of equations for these five variables, we need to impose periodic boundary condition within two cells, i.e., $P_0=F_1(0)=F_1(2l)$. The resulting equation set admits solutions with both spatial periods, l and $2l$. A detailed discussion of this point will be reported elsewhere.

The symmetry-breaking mechanism discussed here consists in the irregular accumulation of particles in some substrate wells, with the remaining wells getting completely depleted. This occurs via the amplification of fluctuations: very minor, random differences in particle occupation of different cells become more and more pronounced when time evolves

and finally break the original equivalence of all cells. This is somewhat similar to the "Maxwell demon" mechanism where particles originally equally distributed among cells accumulate in some wells while depleting other wells. Also, it provides a deep analogy between this nonequilibrium dynamics near the condensation point and dynamical instabilities or critical fluctuations near symmetry-breaking phase transitions (see, e.g., Ref. [21]). For instance, critical fluctuations at the critical temperature produce a symmetry-broken ferromagnetic state (with either up or down magnetization along a ferromagnetic easy-axis) from a fully symmetric paramagnetic phase [Fig. 10(a)]. By analogy, if two particles start their motion from an unstable equilibrium position, they can move far apart from one another, depending on very minor differences in their initial conditions [Fig. 10(b)]. Note that such an analogy between equilibrium phase transitions and instability of dynamical systems has been successfully used in the renormalization-group approach. Moreover, spontaneous symmetry breaking in closed ratchet chains can be observed in a variety of quasi-1D physical systems (e.g., [4]), including the simple experimental setup sketched in Fig. 10(c).

CONCLUSION

In conclusion, the transport of interacting particles in a rocked ratchet was studied both analytically and numerically. The ratchet current can increase or decrease with the density for both attracting and repulsive interparticle interactions depending on the temperature and the ac drive. Most notably, for certain values of the drive and temperature, attracting particles can condense at a subset of the potential minima. Depending on the drive amplitude, condensation may result in either a drop of the net velocity to zero or in its saturation for high densities. Under the latter circumstances, a very efficient rectification mechanism sets in. These findings provide new methods for controlling transport of small particles in complex biological systems and in nano- or microdevices.

[1] See, e.g., the following reviews: P. Reimann, Phys. Rep. **361**, 57 (2002); R. D. Astumian and P. Hänggi, Phys. Today **55** (11), 33 (2002); F. Julicher, A. Ajdari, and J. Prost, Rev. Mod. Phys. **69**, 1269 (1997); R. D. Astumian, Science **276**, 917 (1997); J. M. R. Parrondo and B. J. De Cisneros, Appl. Phys. A: Mater. Sci. Process. **75**, 179 (2002).

[2] D. A. Doyle, J. M. Cabral, R. A. Pfuetzner, A. Kuo, J. M. Gulbis, S. L. Cohen, B. T. Chait, and R. MacKinnon, Science **280**, 69 (1998).

[3] K. Kitamura, M. Tokunaga, A. H. Iwane, and T. Yanagida, Nature (London) **397**, 129 (1999).

[4] For reviews, see: the special issue in Appl. Phys. A: Mater. Sci. Process. **75**, 169 (2002) on *Ratchets and Brownian Motors: Basics Experiments and Applications*, edited by H. Linke; and the issue in Chem. Phys. **281**, 167 (2002) on *Transport in Molecular Wires*, edited by P. Hanggi, M. Ratner, and S. Yaliraki.

[5] J. E. Villegas, S. Savel'ev, F. Nori, E. M. Gonzalez, J. V. Anguita, R. García, and J. L. Vicent, Science **302**, 1188 (2003).

[6] S. Matthias and F. Muller, Nature (London) **424**, 53 (2003).

[7] Z. Siwy and A. Fuliński, Phys. Rev. Lett. **89**, 198103 (2002); C. Marquet, A. Buguin, L. Talini, and P. Silberzan, *ibid.* **88**, 168301 (2002).

[8] P. T. Korda, M. B. Taylor, and D. G. Grier, Phys. Rev. Lett. **89**, 128301 (2002); B. A. Koss and D. G. Grier, Appl. Phys. Lett. **82**, 3985 (2003).

[9] R. Bartussek, P. Hänggi, and J. P. Kissner, Europhys. Lett. **28**,

459 (1994); M. O. Magnasco, Phys. Rev. Lett. **71**, 1477 (1993).

[10] B. Y. Zhu *et al.*, Phys. Rev. B **68**, 014514 (2003); Physica E (Amsterdam) **18**, 322 (2003); **18**, 318 (2003); Phys. Rev. Lett. **92**, 180602 (2004); F. Marchesoni *et al.*, Physica A **325**, 78 (2003); J. F. Wambaugh *et al.*, Phys. Rev. Lett. **83**, 5106 (1999); C. J. Olson *et al.*, *ibid.* **87**, 177002 (2001).

[11] F. Marchesoni, Phys. Rev. Lett. **77**, 2364 (1996); P. Reimann *et al.*, Europhys. Lett. **45**, 545 (1999).

[12] A hard-rod gas on a flashing ratchet was studied by I. Derényi and T. Vicsek, Phys. Rev. Lett. **75**, 374 (1995).

[13] J. Buceta, J. M. Parrondo, C. Van den Broeck, and F. J. de la Rubia, Phys. Rev. E **61**, 6287 (2000).

[14] C. Van den Broeck, I. Bena, P. Reimann, and J. Lehmann, Ann. Phys. (Leipzig) **9**, 713 (2000).

[15] P. Reimann, R. Kawai, C. Van den Broeck, and P. Hänggi, Europhys. Lett. **45**, 545 (1999).

[16] C. Van den Broeck, J. M. R. Parrondo, and R. Toral, Phys. Rev. Lett. **73**, 3395 (1994).

[17] J. H. Morais-Cabral, Y. Zhou, and R. MacKinnon, Nature (London) **414**, 37 (2001).

[18] S. Savel'ev, F. Marchesoni, and F. Nori, Phys. Rev. Lett. **91**, 010601 (2003); **92**, 160602 (2004).

[19] S. Savel'ev, F. Marchesoni, and F. Nori, Phys. Rev. E **70**, 061107 (2004).

[20] C. Van den Broeck, J. M. R. Parrondo, J. Armero, and A. Hernández-Machado, Phys. Rev. E **49**, 2639 (1994).

[21] S. Savel'ev and F. Nori, Phys. Rev. B **70**, 214415 (2004).